Supplemental Data

Multiple Protein Phosphatases Are Required for Mitosis in *Drosophila*

Feng Chen, Vincent Archambault, Ashok Kar, Pietro Lio, Pier Paolo D'Avino, Rita Sinka, Kathryn Lilley, Ernest D. Laue, Peter Deak, Luisa Capalbo, and David M. Glover

Supplemental Experimental Procedures

Double-Stranded RNA Synthesis

A set of 117 genes encoding PPs and their regulatory subunits was defined based on previous reports [S1] and from consultation of Flybase annotations (http://flybase.bio.indiana.edu/). *Drosophila* genomic/cDNA fragments were used for making dsRNA as previously described [S2]; the average length of dsRNA was 500 bp. Gene-specific primers were designed by a custom-made oligonucleotide design program (Philasys [Sysarris]). Each dsRNA sequence was proof-checked individually by blasting against the predicted genes in the *Drosophila* genome for achieving the minimum degree of sequence similarity to other genes and thus controlling false positives. The entire list of these 117 genes and their corresponding primers can be found in Table S4. dsRNAs were subjected to gel electrophoresis for quantification of material and for ensuring that the dsRNA migrated as a single band.

Mitotic-Index Measurement

Cells were fixed in 96-well plates, stained with anti-phosphohistone H3 (Upstate Biotechnology) for visualization of mitotic chromosomes and Hoechst for visualization of total DNA, then imaged by an inverted automated fluorescence microscope (Zeiss Axiovert 200M). For each protein, approximately 200,000 total cells from 6 wells of 96-well plates were screened. The frequency of mitotic cells was calculated by automated image analysis with MetaMorph software (Molecular Devices) and was followed by statistical analysis with a Kolmogorov-Smirnov (K-S) test (see Statistical Analysis). At least two independent experiments were performed for each dsRNA.

Quantitative Assessment of Mitotic Defects

Cells were fixed on glass coverslips and stained with anti-γ- and α-tubulin antibodies and DAPI for visualizing centrosomes, microtubules, and chromosomes. Coded numbers were assigned to control and sample slides, and mitotic defects were counted blindly. At least 200 mitotic cells were scored per slide with a Zeiss Axiovert 200M microscope. For quantifying the defect in mitotic progression, cells were grouped into four mitotic stages (prophase, prometaphase + metaphase, anaphase, and telophase), after which the percentage of cells in each stage relative to the total number of mitotic cells was calculated. For determining the morphological defects, defective mitotic cells were assigned to one or more of 20 categories of morphological abnormality, coded to facilitate computer analysis of the data (Table S2). These defects were then grouped into three classes including centrosome, spindle, and chromosome defects, and the proportion of cells with each class of these defects was calculated relative to the total number of mitotic cells. The severity of a specific mitotic defect was ranked by the Z score. On the basis of control values from 20 *GFP* RNAi experiments, 99.7% confidence intervals ($-3 < Z < 3$) were defined.

Statistical Analysis

Kolmogorov-Smirnov Test

Mitotic indices were analyzed with the Kolmogorov-Smirnov (K-S) test for determining whether the dataset of sample RNAi significantly differ from the dataset of *GFP* RNAi (control). This test has the advantage of making no assumption of data distribution; i.e., it is nonparametric and distribution free. For each dsRNA, two independent experiments were carried out, and in each experiment, we used two *GFP* RNAi controls to increase the accuracy. We first tested and confirmed that the two *GFP* RNAi controls always displayed very similar distributions, indicating we were able to replicate the experimental conditions. We then tested the effect of a series of sample RNAi experiments, $F_1(x)$, against the effect of both *GFP* RNAi experiments, $F_2(x)$. The null hypothesis for this test is that the two datasets are drawn from the same continuous distribution. The alternative hypothesis is that they are drawn from different continuous distributions. The test statistics is $\max|F_1(x) - F_2(x)|$, and the null hypothesis is rejected at a 0.01 level of significance. Table 1 provides the list of genes whose downregulation showed significantly different distributions from *GFP* RNAi controls in both screens involving distinct dsRNAs (we also report alongside each gene name the average K-S values). We further confirmed our results by using the bootstrap Kolmogorov-Smirnov, which executes a bootstrap version of the Kolmogorov-Smirnov test and is particularly appropriate when the distributions being compared are not entirely continuous. Full details of the test used in this study are described in [S3] and [S4].

Vector Construction

For generating pAc5-TEV/PrA, DNA coding for the calmodulin binding peptide (CBP) followed by the cleavage site for the tobacco etch virus (TEV) protease and two immunoglobulin binding (IgG) domains of *S. aureus* protein A were inserted in frame downstream the V5 epitope in a pAc5.1/V5-HisA vector (Invitrogen) lacking His sequences. Subsequently, a Gateway cassette was introduced between the Actin 5C promoter and the V5/CBP/TEV/ProtA region. For generating a Metallothionein (MT) inducible vector, a KpnI/PmeI fragment from pAc5-TEV/PrA containing the Gateway-V5/CBP/TEV/ProtA cassette was inserted into the respective sites of pMT/V5-His vector (Invitrogen).

Protein A Affinity Purifications

Approximately 5×10^8 cells stably transfected with either pMt-MEI-S332-PrA or pAc5-Zw10-PrA were harvested by centrifugation, washed with PBS containing EDTA-Free Complete protease inhibitors (Roche), and frozen in liquid nitrogen. For inducing expression of pMt-MEI-S332-PrA, cells were incubated overnight with complete medium containing 1 mM $CuSO_4$. Cells were thawed in 5 ml of extraction buffer (50 mM Tris-Cl [pH 7.5], 150 mM NaCl, 2 mM $MgCl_2$, 1 mM EGTA, 0.1% NP-40, 0.5 mg/ml DNase [DN-EP; Sigma], 1 mM DTT, and Complete inhibitors [Roche]) then frozen and thawed once more to help lysis and extraction. Lysates were agitated at 4°C for 30 min and clarified by centrifugation at 12,000 rpm in a SS34 rotor. Two hundred microliters of Dynabeads (Invitrogen) conjugated to rabbit IgG (MP Biochemicals) were added to the supernatants for a 4 hr incubation with agitation at 4°C. Beads were washed five times for 10 min in 10 ml of extraction buffer. Proteins were eluted from the beads with 0.5 M NH_4OH and 0.5 mM EDTA. Eluates were lyophilized and resuspended in Laemmli SDS-PAGE sample buffer (Sigma) and resolved by SDS-PAGE on an 8%–16% Tris-Glycine gel (Invitrogen).

Mass Spectrometry

Proteins within the gel pieces were first reduced, carboxyamidomethylated, and then digested to peptides with trypsin on a MassPrep-Station (Waters). The resulting peptides were applied to a LC-MS/MS. For LC-MS/MS, the reverse-phase liquid chromatographic separation of peptides was achieved with a PepMap C18 reverse phase, 75 mm i.d., 15 cm column (LC Packings) on a capillary LC system (Waters) attached to a QTof2 (Waters) mass spectrometer. The MS/MS fragmentation data achieved was used for searching the National Center for Biotechnology Information database with the MASCOT search engine (http://www.matrixscience.com). Probability-based MASCOT scores were used for evaluating

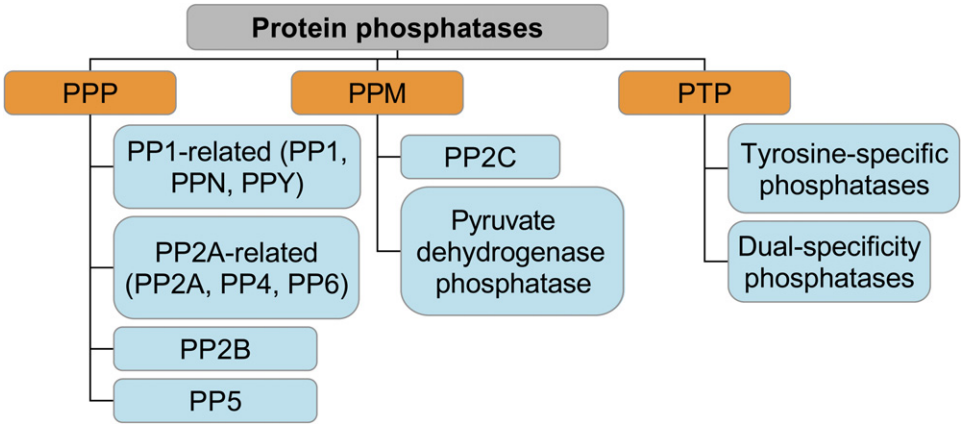

Figure S1. Protein Phosphatase Families and Superfamilies

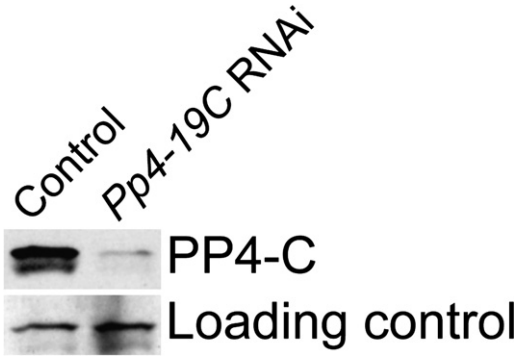

Figure S2. Downregulation of *Pp4-19C* after Its RNAi

Western blot of Pp4-19C (PP4 catalytic subunit) after its RNAi. Control cells were treated with *GFP* dsRNA. Actin was used as a loading control.

identifications. Only matches with $p < 0.05$ for random occurrence were considered significant (further explanation of MASCOT scores can be found at http://www.matrixscience.com).

Determination of the Relative Fluorescence Intensity of MEI-S332

Images of *GFP* (control) and *wdb* RNAi cells were collected with a Zeiss Axiovert 200M microscope with identical exposure time. Single optical sections were taken from a z series of either GFP- or Wdb-depleted cells and subjected to quantification. The equation (S − B)/B was used to compensate for variations in brightness. For determining the signal intensity of MEI-S332 (S), a box of 8 × 8 pixels was placed between each pair of centromeres (as revealed by CID staining; Figure S7, arrows) and the average fluorescence intensity for the channel containing the MEI-S332 signal was measured with the MetaMorph software (Molecular Devices). The contribution of nonspecific background signal (B) was determined by measurement of the average fluorescence intensity with the same box for a region directly adjacent to the metaphase plate (Figure S7, arrowheads).

Antibodies

Full-length CID cDNA and a fragment corresponding to amino acids 244–743 of BubR1 were expressed as histidine-tagged proteins with the pET23b vector (Novagen) in *E. coli*. The products were purified and injected into a chicken and a rabbit (Harlan Sera), respectively. Production of rabbit anti-cyclin B, mouse anti-Polo and T47 mouse anti-Lamin has been described in [S5–S7]. Anti-MEI-S332 [S8] was kindly given by Terry Orr-Weaver (MIT, USA). The following antibodies were purchased from commercial sources: rat anti-tubulin (YL1/2; Oxford Biotechnology), mouse anti-γ-tubulin (GTU88; Sigma), rabbit anti-phosphohistone H3 (Upstate), mouse anti-human PP2A catalytic subunit (Upstate), and sheep anti-human PP4 catalytic subunit (Upstate); the secondary antibodies used for detecting all antigens were conjugated with Rhodamine Red-X, FITC (Jackson ImmunoResearch), or Alexa Fluor 488 (Molecular Probes).

Supplemental References

S1. Morrison, D.K., Murakami, M.S., and Cleghon, V. (2000). Protein kinases and phosphatases in the Drosophila genome. J. Cell Biol. *150*, F57–F62.

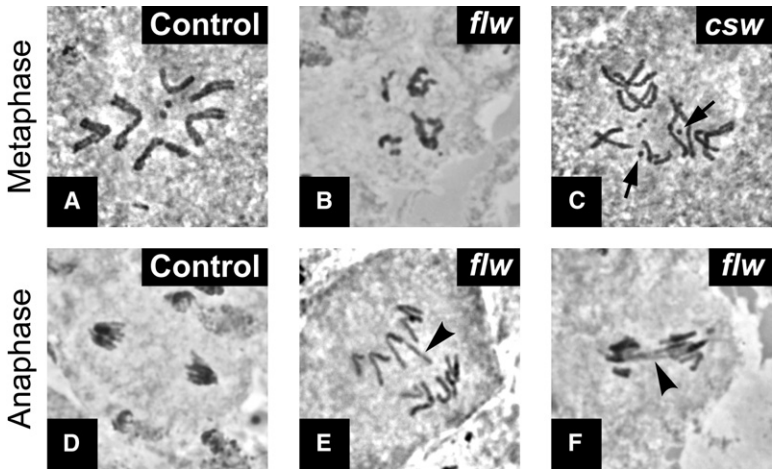

Figure S3. Mitotic Phenotypes of *flw* and *csw* Mutants

Orcein-stained preparations of larval neuroblasts. When compared with the wild-type (A and D), *flw* mutants showed metaphase figures with tangled and unevenly condensed chromosomes (B) and anaphase figures with lagging chromosomes ([E], see arrowhead) and chromosome bridges ([F], see arrowhead); *csw* mutants showed premature sister-chromatid separation ([C], see arrows).

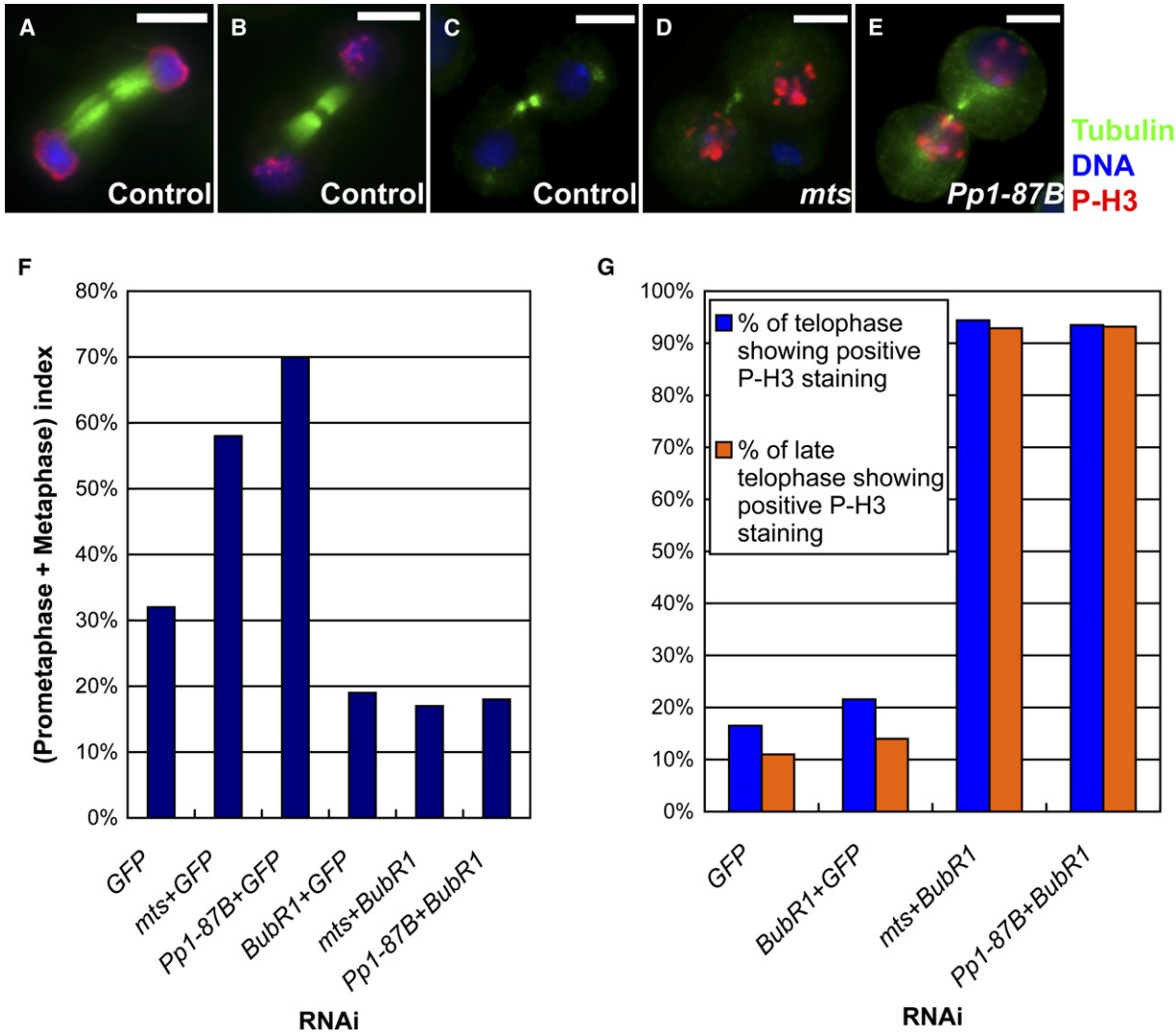

Figure S4. PP2A and Pp1-87B Activities Are Required for Mitotic Dephosphorylation of P-H3

(A–C) In control cells, P-H3 signals began to decrease at early telophase and then disappeared completely at late telophase.

(D–E) RNAi for *mts* (*PP2A-C*) or *Pp1-87B* led to an abnormal accumulation of P-H3 on decondensed chromosomes at late telophase.

(F) Knockdown of BubR1 rescued the prometaphase arrest of cells simultaneously depleted for Mts (PP2A-C) or Pp1-87B. At least 200 mitotic figures were scored for each sample.

(G) P-H3 was still present upon mitotic exit in cells depleted for Mts (PP2A-C) or Pp1-87B. At least 100 telophase figures were scored for each sample. A total amount of 30 μg dsRNA was used for each simultaneous RNAi experiment. *GFP* dsRNA was used to compensate the total amount of dsRNA transfected into cells. Scale bars in (A)–(E) represent 5 μm.

S2. Bettencourt-Dias, M., Sinka, R., Frenz, L., and Glover, D.M. (2005). RNAi in Drosophila cell cultures. In Gene Silencing by RNA Interference: Technology and Application, M. Sohail, ed. (Boca Raton, FL: CRC Press LLC), pp. 147–166.

S3. Chakravarti, I., Laha, R., and Roy, J. (1967). Handbook of Methods of Applied Statistics, *Volume 1* (New York: John Wiley and Sons).

S4. Press, W.H., Teukolsky, S.A., Vetterling, W.T., and Flannery, B.P. (1992). Numerical Recipes in FORTRAN: The Art of Scientific Computing, Second Edition (Cambridge: Cambridge University Press).

S5. Whitfield, W.G., Gonzalez, C., Maldonado-Codina, G., and Glover, D.M. (1990). The A- and B-type cyclins of Drosophila are accumulated and destroyed in temporally distinct events that define separable phases of the G2-M transition. EMBO J. *9*, 2563–2572.

S6. Llamazares, S., Moreira, A., Tavares, A., Girdham, C., Spruce, B.A., Gonzalez, C., Karess, R.E., Glover, D.M., and Sunkel, C.E. (1991). polo encodes a protein kinase homolog required for mitosis in Drosophila. Genes Dev. *5*, 2153–2165.

S7. Paddy, M.R., Belmont, A.S., Saumweber, H., Agard, D.A., and Sedat, J.W. (1990). Interphase nuclear envelope lamins form a discontinuous network that interacts with only a fraction of the chromatin in the nuclear periphery. Cell *62*, 89–106.

S8. Tang, T.T., Bickel, S.E., Young, L.M., and Orr-Weaver, T.L. (1998). Maintenance of sister-chromatid cohesion at the centromere by the Drosophila MEI-S332 protein. Genes Dev. *12*, 3843–3856.

S9. Bjorklund, M., Taipale, M., Varjosalo, M., Saharinen, J., Lahdenpera, J., and Taipale, J. (2006). Identification of pathways regulating cell size and cell-cycle progression by RNAi. Nature *439*, 1009–1013.

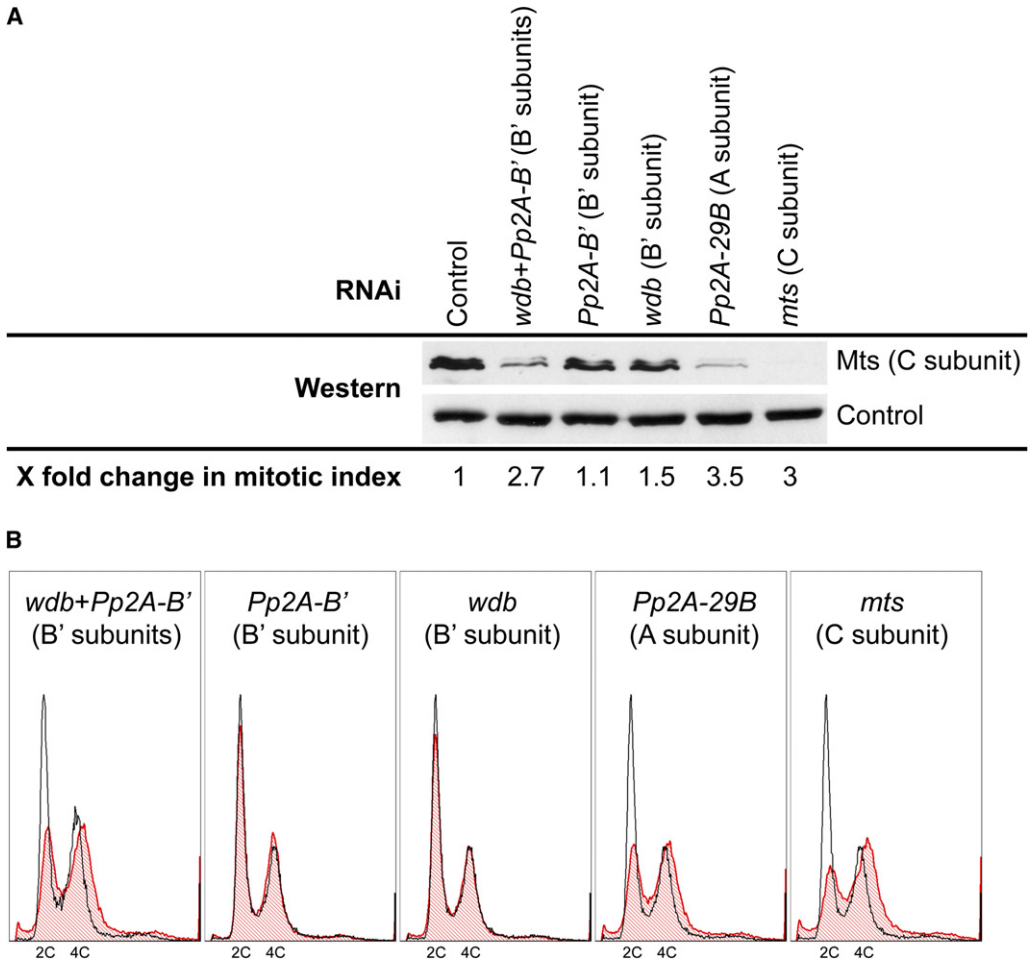

Figure S5. Reduced Stability of PP2A Catalytic Subunit (Mts) after Knockdown of PP2A Scaffolding A Subunit and Simultaneous Knockdown of Both PP2A B' Regulatory Subunits

(A) Western blot of Mts (catalytic C subunit) after RNAi knockdown of Mts, Pp2A-29B (scaffolding A subunit), Wdb or Pp2A-B' (regulatory B' subunits), and simultaneous RNAi for *wdb* and *Pp2A-B'*. Control cells were treated with *GFP* dsRNA. Actin was used as a loading control. Corresponding standardized mitotic indices are listed beneath western-blot tracks. Note that the level of Mts was substantially reduced after the RNAi for *Pp2A-29B* or simultaneous RNAi for *wdb* and *Pp2A-B'*. RNAi for either *wdb* or *Pp2A-B'* alone did not significantly affect Mts stability.
(B) Flow-cytometric histograms after downregulation of indicated PP2A phosphatases are shown in red. Control profiles (cells transfected with dsRNA for GFP) are shown in black. Note that the severity of both flow-cytometric profile and mitotic-index phenotypes are related to the level of Mts shown on the western blot. We also noted that there was a slight but consistent shift of cells from 2C to 4C after knockdown of the either B' subunit (Wdb and Pp2A-B').

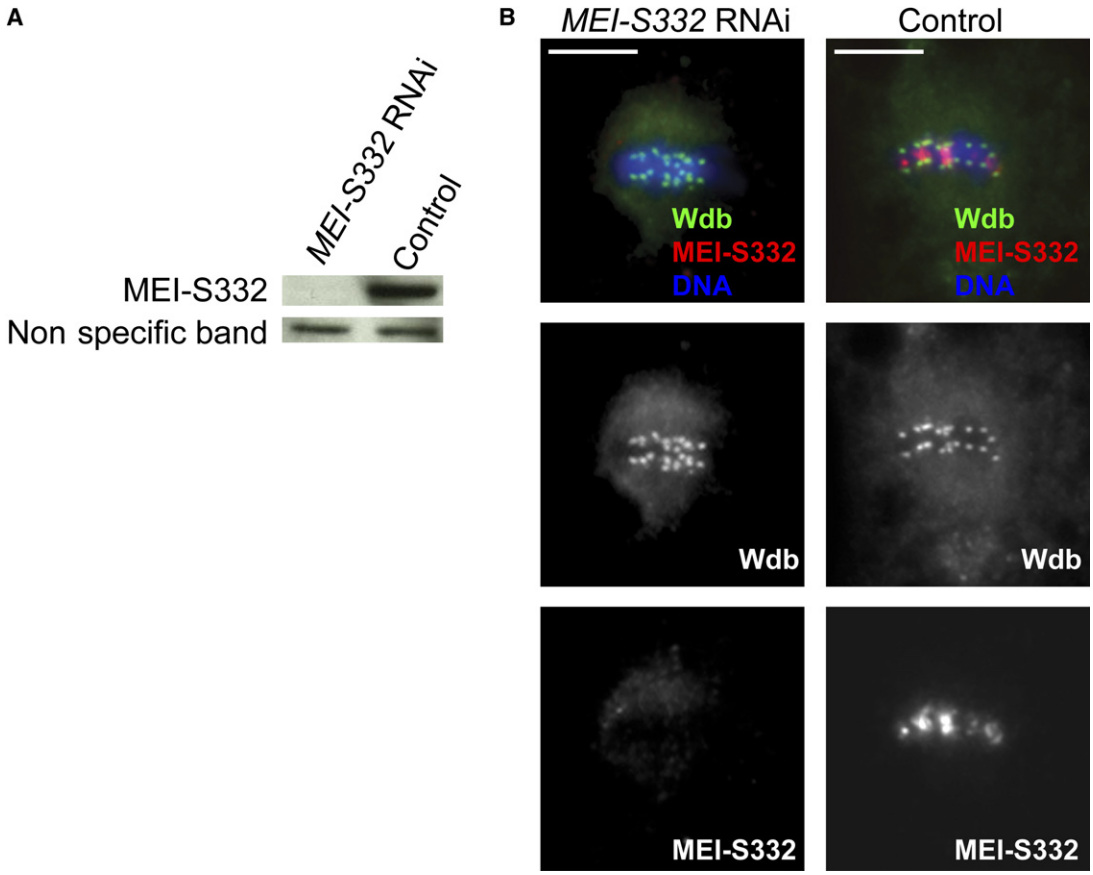

Figure S6. Depletion of MEI-S332 Did Not Affect the Normal Localization of Wdb

(A) Western blot showing that MEI-S332 protein was efficiently depleted after 4 days of RNAi. Note that an equal amount of total proteins was loaded as suggested by the similar protein level of a nonspecific band recognized by the anti-MEI-S332.
(B) The normal localization of Wdb was not changed after depletion of MEI-S332. Note the absence of MEI-S332 staining on the metaphase chromosomes after its RNAi knockdown. Scale bars represent 5 μm.

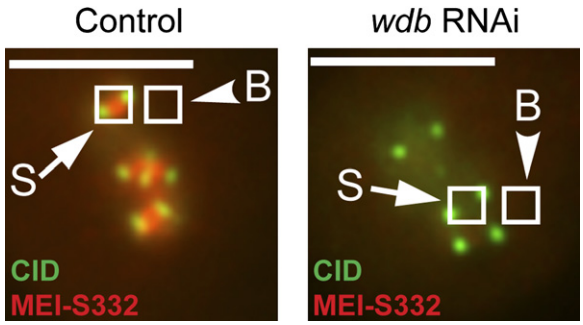

Figure S7. Illustration of the Method Used to Determine the Relative Fluorescence Intensity of MEI-S332

To determine the signal intensity of MEI-S332 (S), a box of 8 × 8 pixels (indicated by arrows) was drawn and placed between the centromeres as revealed by staining for the centromeric marker CID, and the average fluorescence intensity was measured. The same box was then placed directly adjacent to the metaphase plate in a chromosome-free region to measure nonspecific "background" fluorescence ([B], see arrowheads). See Supplemental Experimental Procedures for details. Scale bars represent 5 μm.

Table S1. Confirmation of Phenotypic Effects with Multiple dsRNAs

Gene Name	Flow Cytometry	Mitotic Index
Pp1-87B		
flw		
*sds22**		
*l-t**		
*PpY-55A**		
mts		
Pp2A-29B		
wdb		
tws		
Pp4-19C		
PPP4R2r		
PPV		
*CanA-14F**		
PpD3		
CG1906		
*CG12169**		
CG9311		
*Ptp69D**		
*Ptp99A**		
csw		
Ptp61F		
PTP-ER		
ssh		
puc		

Table S1. *Continued*

Gene Name	Flow Cytometry	Mitotic Index
myotubularin		
sbf		
CG3530		
Pten		
stg		

Flow-cytometry profiles and mitotic indices were tested with a second set of dsRNAs targeting a distinct region of each positive candidate identified in our first screen. In most of the cases, similar phenotypes were observed in both screens (indicated with solid green rounded rectangle). In a few cases, RNAi led to a phenotype in the first but not in the second screen (indicated with half-green-and-half-black rounded rectangle). A solid black rounded rectangle indicates RNAi leading to no phenotype in both screens, and asterisks indicate PPs discarded from further analysis. A large-scale RNAi screen based solely on flow cytometry in *Drosophila* S2 cells has also recently been published [S9]. Only six PPs (*stg*, *puc*, *Pp4-19C*, *Pp1-87B*, *flw*, and *Pten*) were identified in both studies, suggesting that there may be a large number of false positives or negatives in one or both of the screens. Our study was based on a combined analysis of two different phenotypic effects (flow cytometry and mitotic index) and used two nonoverlapping dsRNAs for each candidate identified. It is therefore less prone to identify false positives. Several PPs (*twe*, *Pp1α-96A*, *CG3632*, *CG14211*, and *Lar*) identified by Bjorklund et al. [S9] did not show any significant change in either the flow-cytometry profile or mitotic-index analysis in our study. To investigate this difference, we analyzed the flow-cytometry phenotypes by using the dsRNA library used by Bjorklund et al. [S9], but nevertheless failed to detect any change in the flow-cytometry profile (data not shown).

Table S2. Parameters and Corresponding Codes Used for Quantitation of Mitotic Defects

	Description of Phenotype	Defect Code
Centrosomal Defects		
	Centrosome number zero	CN0
	Single centrosome	CN1
	Centrosome number high (3–5)	CNH
	Centrosome number very high (>5)	CNVH
	Centrosome position defects	CPD
Spindle Defects		
	Monopolar	SMO
	Tripolar	STR
	Multipolar	SMP
	Multipolar cytokinesis	MC
	Abnormal	AS
	Branched	SBR
	Splayed pole	SSP
	No astral microtubules	NAS
	Central spindle defects	CSD
Chromosome Defects		
	Chromosome condensation defect	CRCD
	Chromosome number high	CRNH
	Lagging chromatids	CRLC
	Chromosome alignment defect	CRAD
	Chromosome segregation defects	CRSD
	Unevenly divided DNA	UD